Evolution of crystalline orientations in the production of ferritic stainless steel

IOP Conf. Series: Materials Science and Engineering **891** (2020) 012019 doi:10.1088/1757-899X/891/1/012019

Evolution of crystalline orientations in the production of ferritic stainless steel

A Núñez Galindo[1,3], I Collado Garcia[2], D L Sales[3] and J F Almagro Bello[1]

[1] Acerinox Europa S.A.U, Departamento Técnico / Laboratorios e Investigación, Pol. Industrial Palmones s/n, 11379 Los Barrios, Spain
[2] Universidad de Cádiz, Escuela Superior Ingeniería, Departamento de Ciencia de los Materiales e Ingeniería Metalúrgica y Química Inorgánica, LABCYP Group, Avda. Universidad de Cádiz 10, 11519 Puerto Real, Spain
[3] Universidad de Cádiz, Escuela Politécnica Superior, Departamento de Ciencia de los Materiales e Ingeniería Metalúrgica y Química Inorgánica, INNANOMAT Group, Avda. Ramón Puyol s/n, 11202 Algeciras, Spain

E-mail: andres.nunez@acerinox.com

Abstract. Ferritic stainless steel EN 1.4016 is used in a wide range of applications, the most common ones related to sheet forming. Several problems in the post-processing of these steels relates to their texture and anisotropy. Therefore, it is necessary to know the mechanisms of texture formation in the subsequent stages of metal manufacturing processes. EBSD has been demonstrated as a successful characterisation technique for this purpose.
It is known that during re-crystallisation of Fe-Cr steels, deviations from the desired γ-fibre texture promote a decrease of deep drawability. Additionally, α-fibre damages formability. Subsequent cold rolling and annealing can enhance the deep drawing properties of the steel sheet.
In this research, a standard sample and a modified one with optimised settings as regard to chemical composition and manufacturing process, to improve the formability properties, are characterised. To analyse the preferred orientation and the type of main fibre present in the material, ODF and Aztec Reclassify Phase, to calculate the content of martensite, were used.

1. Introduction

Ferritic stainless steel, in comparison to austenitic one, is low-cost, price-stable and has good engineering properties. Type EN 1.4016 (AISI 430) is used in a large range of applications, including the most common related to conformation, stretching and deep drawing. Recent research evaluates its application as a hydrogen container [1].

Several problems after each rolling and annealing processes during these steels manufacturing, lead to certain preferred crystallographic orientations (coming from their texture). Due to the impact that crystallographic texture has on the anisotropy of material properties, it is necessary to know the mechanisms that are involved in the texture of these materials during its manufacturing routing [2-10]. In this sense, deviations from the γ-fibre desired texture occur during re-crystallisation of Fe-Cr steels, and a large number of grains being oriented with their {111}-plane parallel to the sheet plane, hence promoting a decrease of deep drawability. In the same way, the α-fibre texture component transforms in such a way that <110> orientates parallel to rolling direction and {001}, damaging to formability [11-20].

The orientation measurement of polycrystalline grains (γ- and α-fibre), carried out after formability of the material, allows for evaluation of the deformation mechanism of the material. To describe crystallographic textures, a representation in a three-dimensional space is necessary. This representation is done by maps or diagrams of the orientation distribution function, ODF, defined by Euler angles φ_1, Φ, φ_2, which applied to the axes [100], [010] and [001] of the crystal structure of the grain, make it coincide with the axes RD (rolling direction), ND (normal direction) and TD (transversal direction) of the sample, respectively. In addition, the anisotropic behaviour of flat products can be characterised by the Lankford coefficients; high values of normal plastic anisotropy, r_m (greater than 1), and planar plastic anisotropy, Δr (as close to zero as possible), are good indicators of high formability [21-24].

Texture in steel depends, among other variables, on chemical composition, the remains of the primary solidification structure in the final product [25-26], and processing parameters like finishing temperature during hot rolling, percentage of cold work reduction, annealing temperature and time. Hot rolling process control can provide favourable textures so that subsequent cold rolling and annealing can enhance the deep drawing properties of the steel sheet.

In this research, two variations of the same grade of ferritic stainless steel have been analysed. One of them, type 0A, has both standard composition and processing route intended for a broad and general scope of applications. The other one, type 1C, features optimised settings in chemical composition and manufacturing process to improve the formability properties.

The technical approach, presented in a preliminary study of this research [27], includes characterisation by field emission gun – scanning electron microscopy to study texture formation, evolution and microstructural phases obtained through different steps of the processing route: casting, intermediate hot rolling, final hot rolling, annealing and pickling after hot rolling, and final annealing after cold rolling. EBSD post-processing procedures were used such as pole figure [28] to characterise the anisotropy of the material, orientation distribution function (ODF) to analyse the preferred orientation and the type of main fibre present in the material, and AZTEC RECLASSIFY PHASE [29-34], to calculate the content of martensite within the ferrite matrix.

2. Experimental procedure

Two EN 1.4016 steel samples with different initial compositions (basic: 0A, and modified: 1C) were taken from the daily production of Acerinox Europa, S.A.U. (www.acerinox.es) in different positions of the processing route: from slabs during casting, from intermediate hot rolling, from material after hot rolling with intermediate annealing and after cold rolling, and final annealing. The samples were subjected to thickness reductions between the different production stages, from slab to intermediate hot rolling by 98 % for both materials, and from this stage until final annealing by 80 % for the basic and by 87 % for the modified sample. In the modified annealing treatment, the processing speed of the materials corresponds to an increase of 20 % in the carry-in time into the furnace as compared with the basic.

The chemical composition of the samples was analysed using conventional techniques, X-ray fluorescence (XRF), spark optical emission (S-OES), and instruments available in a stainless steel factory using a Panalytical Axios Fast XRF spectrometer (www.panalytical.com), an Oblf Qsn 750 (www.oblf.de) and Leco CS 600 and TC 600 analysers (www.leco.com). Also, using the THERMOCALC software (TCW 4 using database TCFE5), the phase diagrams were calculated as a function of temperature in equilibrium conditions [35].

The materials selected for this study are summarised in Table 1, together with their global chemical composition and type of applied annealing. The composition of sample 0A is referred to as “basic” composition, while the sample 1C is a “modified” composition, with lower contents of interstitial elements such as C and N.

Table 1. Composition, annealing treatment and metallurgical properties of the as-supplied materials.

Sample identification	Composition (wt%)	Annealing time
0A	**Basic**: C: 0.050; N: 0.035; Si: 0.35; Cr: 16.3	Short
1C	**Modified**: C: 0.025; N: 0.025; Si: 0.45; Cr: 16.7	Long

The phase diagrams of the studied chemical compositions have been analysed by THERMOCALC software. Figure 1 shows the phase diagram of the basic (0A) and modified (1C) samples characterised by a dual phase ferrite-austenite structure, gamma loop and precipitation of chromium carbide type $M_{23}C_6$.

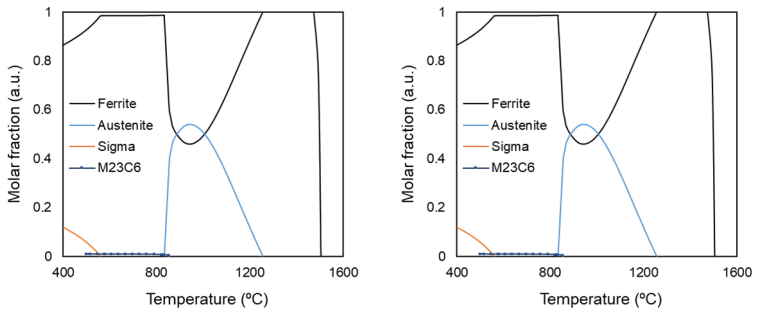

Figure 1. Phase diagrams of the material systems of sample 0A (left) and sample 1C (right).

The phase diagrams show important differences between the two materials in terms of transformation points and amount of high temperature austenite: Ac1 and Ac3 are 855 and 1,256 °C for the 0A material, and 857 and 1,180 °C for the 1C material; while the maximum austenite contents are 53.3 % (at 919 °C) for 0A and 32.8 % (at 943 °C) for 1C. This austenite is not stable so it transforms to martensite when cooling down to room temperature.

Grain size analysis was performed after polishing and etching the samples using Vilella's reagent during 30 to 75 s. The observation and measurement of grain size were performed with an Olympus GX71 light optical microscope (LOM) (www.olympus.co.uk), by Heyn lineal interception and comparison procedures. In order to assess the cooling mechanism of both ferritic stainless steel, electrochemical pickling of the cross-sectional area of the sample is carried out to reveal their macrostructure. As a result, the cooling rate from the surface to the core of each slab is observed [36].

The mechanical tests were carried out in samples with basic and modified composition after hot rolling and after final annealing using a RK100 Roell+Korthaus universal testing machine, for the study of elongation, the average r-value of Lankford and planar anisotropy and coefficient of acrimony.

EBSD characterisation was performed on a Zeiss Ultra 55 FEG-SEM (www.zeiss.es), using polished longitudinal sections of the samples. The sample sections were prepared by conventional metallographic procedures, with a final polish with colloidal silica suspension OPS (www.struers.com). The FEG-SEM used is equipped with a CHANNEL 5 EBSD system, from Oxford Instruments (www.oxinst.com). EBSD maps were acquired at 20 kV, at a working distance of 16 mm and a 0.5 µm step size. In addition, through the EBSD analysis, the software AZTEC RECLASSIFY PHASE, taken into consideration the austenite-ferrite transformation phenomenon, allows to calculate the content of martensite within the ferrite matrix, where ferrite and martensite can be distinguished from each other. The presence of martensite, was then checked by light optical microscopy [37].

3. Results and discussion

3.1. Micro- and macrostructure

Figure 2 shows light optical microscopy (LOM) images of the structure in samples from slabs for basic (0A, left) and modified (1C, right) material, respectively. Optical micrographs of both slab structure show ferritic grains with martensite needles at grain boundaries and within the matrix, as well as the distribution of carbides within the grains is noticeable. Moreover, sub-grains are revealed in the basic composition material (0A) but not in the modified one (1C). Therefore, the structure of material 1C shows a better re-crystallisation state.

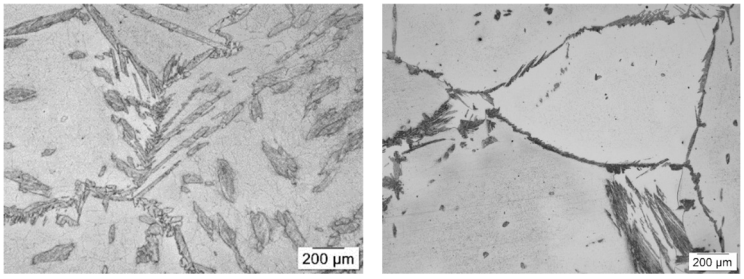

Figure 2. LOM image showing the structure of slab 0A (left) and slab 1C (right).

Figure 3 reveals a detail of the macrostructure of each sample, basic (0A) and modified (1C), in order to study the solidification mechanism of both ferritic stainless steel. The characterisation of the macrostructure indicates that the solidification mechanism is heterogeneous in the material with basic composition, whereas in the modified composition it is homogeneous.

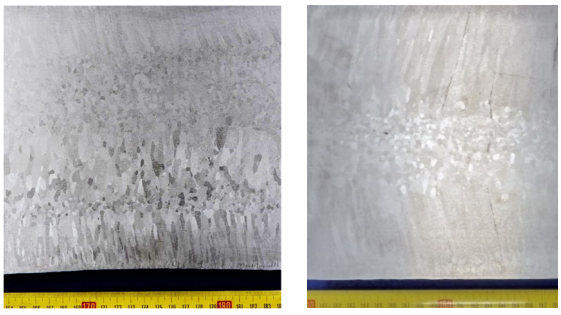

Figure 3. Macrostructure in the basic material 0A (left) and in the modified one 1C (right).

3.2. Mechanical properties

The results of elongation, anisotropy and strain hardening of both hot rolled (HR) and final annealed (FA) materials are shown in Table 2.

Table 2. Summary of mechanical tests.

Sample Id.	A (%)	r-value			r_m	Δr	n
		RD	ND	TD			
0A after HR	31	0.36	0.63	0.48	0.52	-0.21	0.18
1C after HR	28	0.34	0.69	0.54	0.57	-0.25	0.15
0A after FA	28	0.86	0.70	1.18	0.86	0.32	0.21
1C after FA	29	0.80	1.05	1.21	1.17	-0.09	0.21

The average anisotropy (r_m) and the planar (Δr) were calculated by the following equations:

$$r_m = (r_0 + r_{90} + 2r_{45}) / 4 \quad (1)$$
$$\Delta r = (r_0 + r_{90} - 2r_{45}) / 2 \quad (2)$$

The values of normal anisotropy and strain hardening in the hot rolled materials are significantly lower than those of the annealed materials, which is consistent with the corresponding microstructures: deformed and re-crystallised. On the other hand, both normal and planar anisotropy values are clearly more favourable in the 1C material, which means that it has a better performance for deep drawing operations. Therefore, the basic composition sheet exhibits more pronounced anisotropy and lower deep drawability than the modified composition sample.

3.3. Orientation distribution function, pole figures and reclassify phase

EBSD analysis allowed obtaining information of the whole sample thickness for the main phase, as the observation plane was ND-LD (ND and LD stand for normal direction and line, or rolling, direction). The FEG-SEM characterisation was carried out using a polished sample in longitudinal section (ND-LD plane).

To analyse the texture and the most important fibre present in the material, the procedure used is the orientation distribution function (ODF); it is well known that the rolling process reinforces the α-fibre (<110> parallel to RD, at Φ = 0°) and re-crystallisation reinforces the γ-fibre (<111> parallel to ND, at Φ = 55°). The pole figures, where random texture indicates uniform distribution in the projection, elements of symmetry for each plane can be analysed and so the anisotropy of the material.

Texture, anisotropy and content of martensite is analysed in basic (0A) and modified (1C) materials at different steps of the processing route: during hot rolling and after intermediate and final annealing.

3.3.1. Samples intermediate hot rolling

Figure 4 shows the ODF of basic and modified material in samples before final hot rolling with a thickness of 26 mm. EBSD texture results indicate the presence of γ-fibre in the modified material (Fig. 4-left) for the presence of density at Φ = 55°, and the absence of γ-fibre at Φ = 55° in the basic one (Fig. 4-right) where α-fibre predominates.

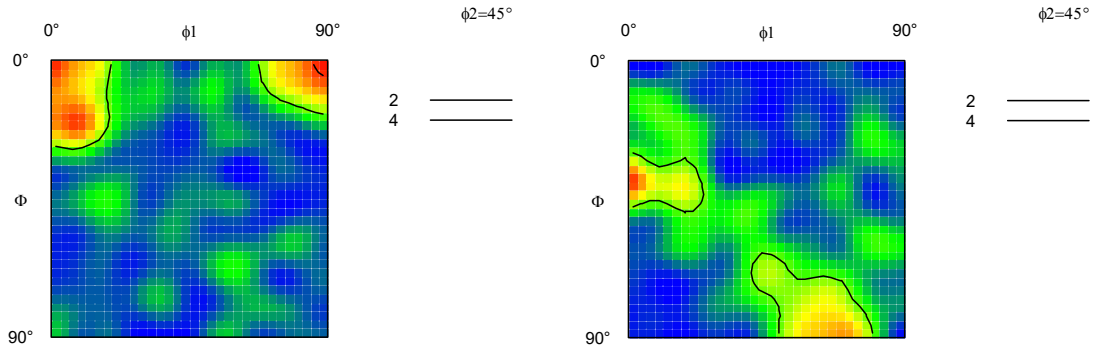

Figure 4. ODF of basic material, 0A (left) and modified material, 1C (right), before final hot rolling.

Figure 5 shows the pole figure of basic and modified material in samples during hot rolling, before finishing mill. Pole figures indicate that symmetry elements for each plane, in both materials, are not clearly defined, probably because, in this state, the materials have not developed its ideal orientations that can be found in bcc materials [28].

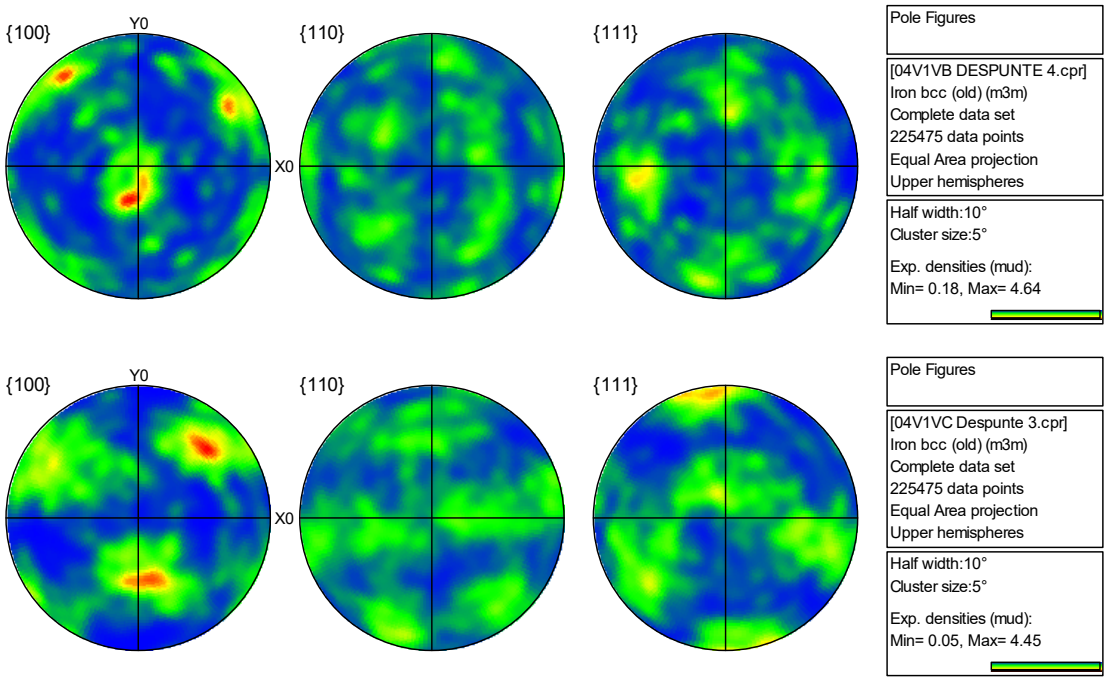

Figure 5. Above: pole figure of basic material, 0A, before final hot rolling. Below: pole figure of modified material, 1C, before final hot rolling.

Figure 6a shows the band contrast (BC), coincidence site lattice CSL) and grain boundaries (GB) map, Fig. 6b shows the CSL legend, while Fig. 6c shows the GB legend, of the basic and the modified material in samples during hot rolling before finishing mill.

The characterisation reveals the presence of a phase in the ferrite matrix (red areas in images), identified as retained martensite after quenching, in both materials [28]. Martensite and ferrite cannot be discriminated by EBSD and this software uses the density of crystalline defects to identify the martensite areas, as follows: the tetragonal elongation is greater than 2.5 - 3 % between a-, b- and c-axes, Fig. 7. This means that there is a real chance to separate martensite from Fe bcc as shown in reference [30]; in this case it would be > 3 % (3 % = 2.93138 c-axis). The specific algorithm to solve pattern is using mentioned in references [30] and [33-34]. Using martensite structure data means that it is possible recognise and index martensite in a range greater than 3 % tetragonal distortion. The content of this martensite is 27 % in basic material and 11 % in the modified one, so the content of retained martensite that corresponds to the previous austenite transformed during hot rolling is higher in basic material and, therefore, texture formation will also be higher.

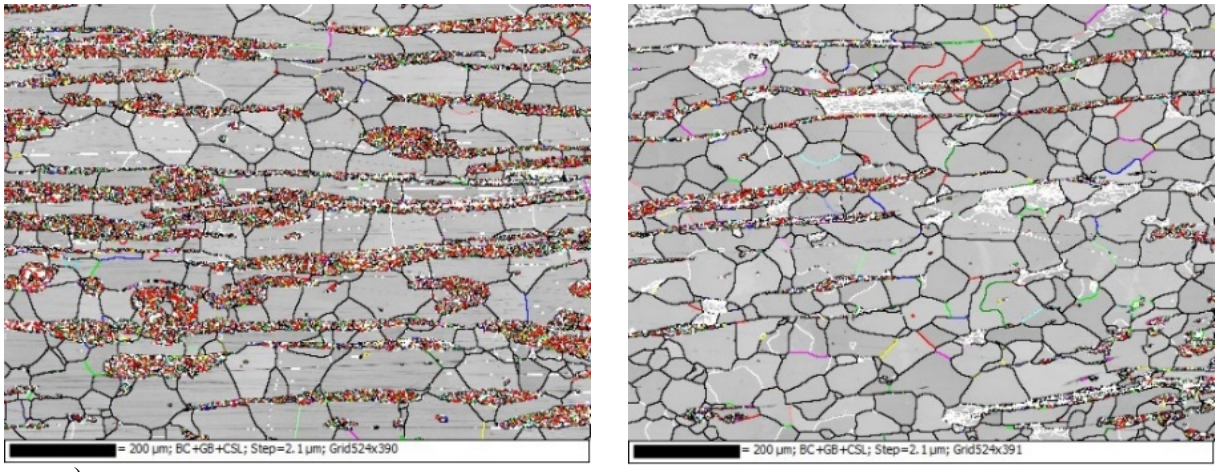

a)

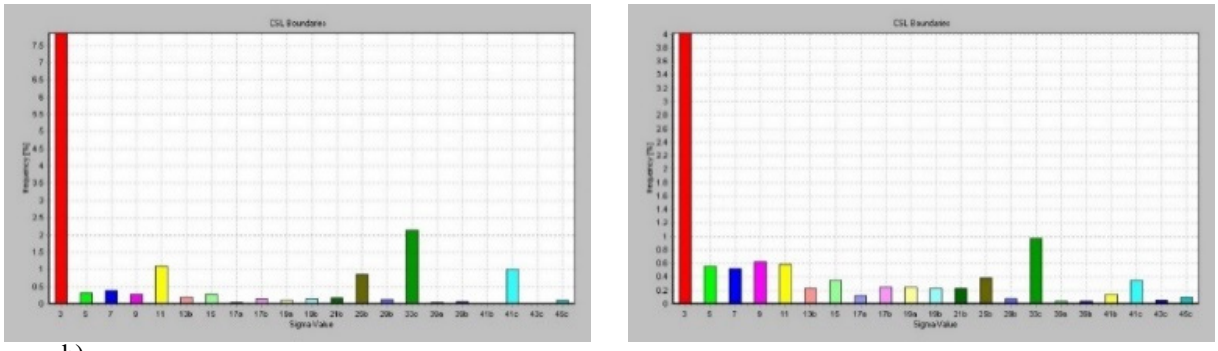

b)

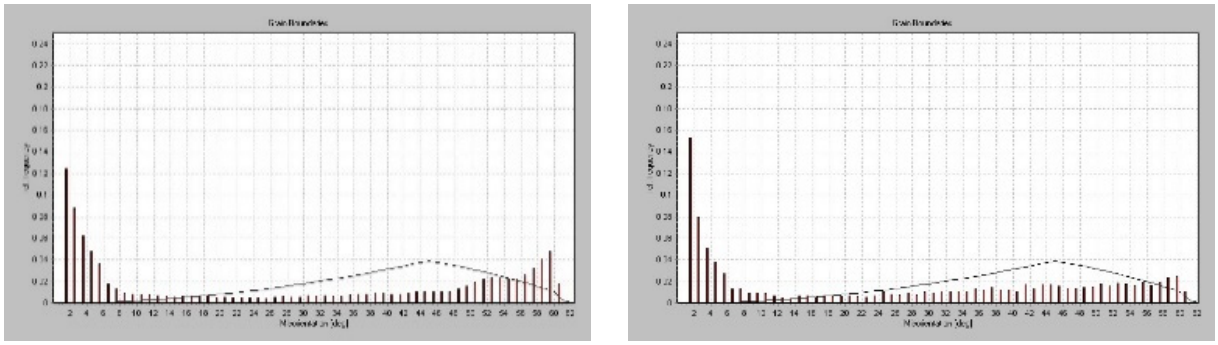

c)

Figure 6. a) Band contrast (BC), coincidence site lattice (CSL) and grain boundary (GB) map of basic material, 0A (left) and modified material, 1C (right) during hot rolling. b) CSL legend of basic (left) and modified (right) material in samples during hot rolling. c) GB legend of basic (left) and modified (right) material in samples during hot rolling.

Fe bcc

Crystal system:	Cubic
Space group:	I m -3 m
Space group number:	229
a (Å):	2.8710
b (Å):	2.8710
c (Å):	2.8710
Alpha (°):	90.0000
Beta (°):	90.0000
Gamma (°):	90.0000
Calculated density (g/cm^3):	7.83
Volume of cell (10^6 pm^3):	23.66
Z:	2.00
RIR:	11.07

Martensite

Crystal system:	Tetragonal
Space group:	I4/mmm
Space group number:	139
a (Å):	2.8460
b (Å):	2.8460
c (Å):	3.0530
Alpha (°):	90.0000
Beta (°):	90.0000
Gamma (°):	90.0000
Calculated density (g/cm^3):	7.09
Volume of cell (10^6 pm^3):	24.73
Z:	1.00
RIR:	7.36

Figure 7. Fe bcc and martensite crystallographic parameters; ICSD (Inorganic Crystal Structure Database) pattern.

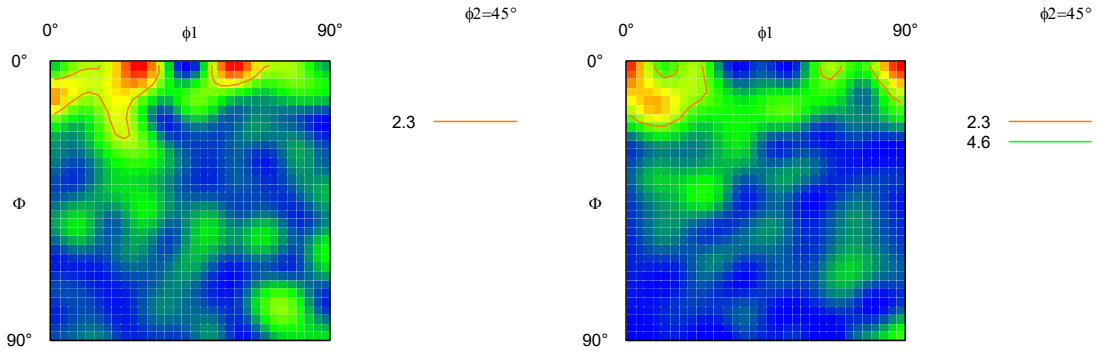

Figure 8. ODF of basic material, 0A (left), and modified material, 1C (right) with intermediate annealing.

3.3.2. Samples with intermediate annealing, after hot rolling. Figure 8 shows the ODF of basic and modified material with intermediate annealing, after hot rolling. ODFs indicate that α-fibre prevails in both materials, and that γ-fibre is not observed in either.

Figure 9 shows the pole figure of basic and modified material in samples after hot rolling. Pole figures indicate that components of re-crystallised austenite upon transformation to ferrite seem to be observed mainly in material 0A [28].

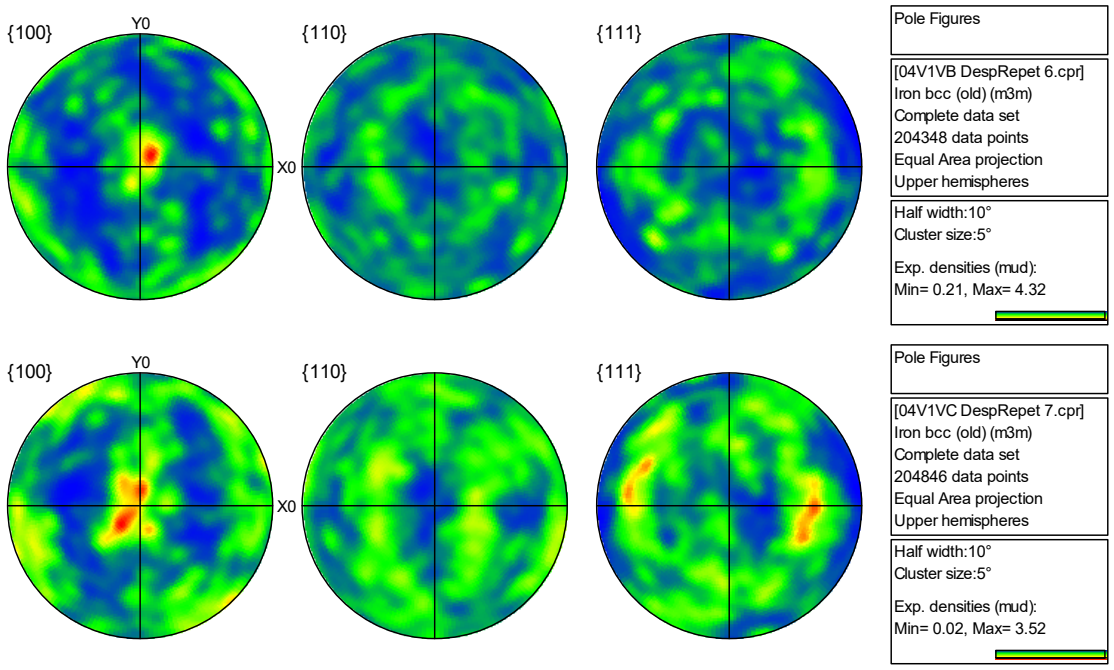

Figure 9. Above: pole figure of basic material, 0A, after hot rolling and its corresponding annealing. Below: pole figure of modified material, 1C, after hot rolling and its corresponding annealing.

Figure 10a shows the band contrast (BC), coincidence site lattice (CSL) and grain boundaries (GB) map, Fig. 10b shows the CSL legend, while Fig. 10c shows the GB legend of basic and modified material after hot rolling plus annealing. Data processing has been performed as it was done for the samples during hot rolling (Fig. 6). EBSD analysis does not show the presence of retained martensite in the ferritic matrix in any of the materials after hot rolling; also, a poor re-crystallisation in the modified material is observed.

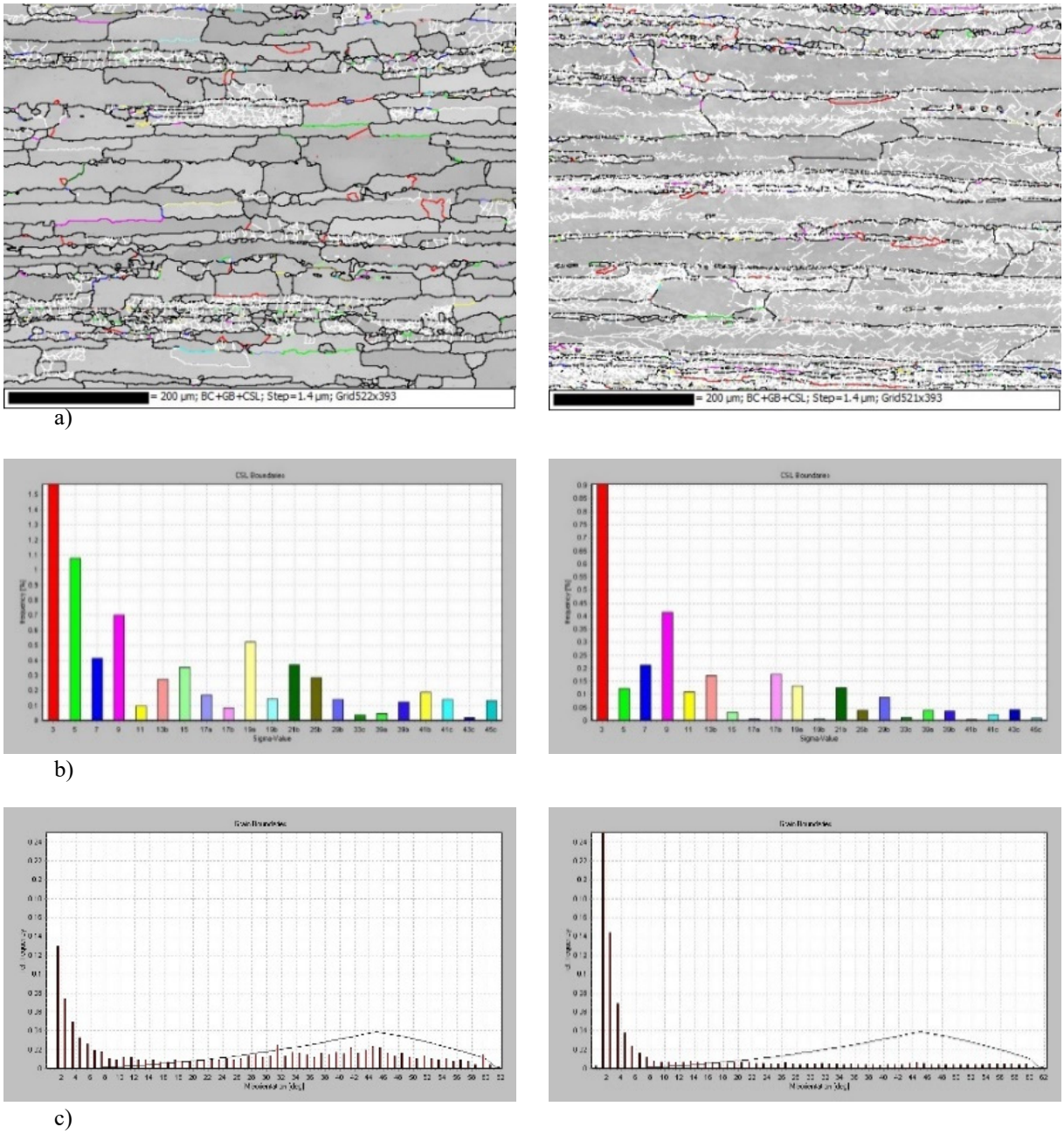

Figure 10. a) Band contrast (BC), coincidence site lattice (CSL) and grain boundary (GB) map of basic material, 0A (left) and modified material, 1C (right) after hot rolling and its corresponding annealing. b) CSL legend of basic (left) and modified (right) material in samples during hot rolling. c) GB legend of basic (left) and modified (right) material after hot rolling and its corresponding annealing.

3.3.3. Samples after cold rolling and final annealing. Figure 11 shows the ODF of basic and modified material in samples after cold rolling and final annealing. A strong γ-fibre re-crystallisation texture is developed in the modified steel after cold rolling and final annealing, while α-fibre was mostly found in the basic one.

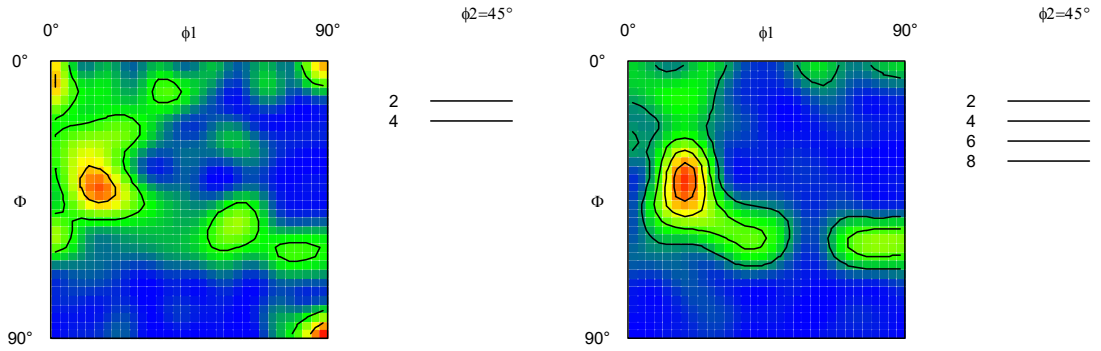

Figure 11. ODF of basic material, 0A (left), and modified material, 1C (right) after cold rolling and final annealing.

Figure 12 shows the pole figure of basic and modified material after final annealing. It is observed that in the material 0A, symmetry elements distribution in the projection is not uniform, but in the 1C material symmetry, elements are observed for each plane, texture components in cold-rolled and re-crystallised BCC steels; so the material of basic composition, presents higher anisotropy.

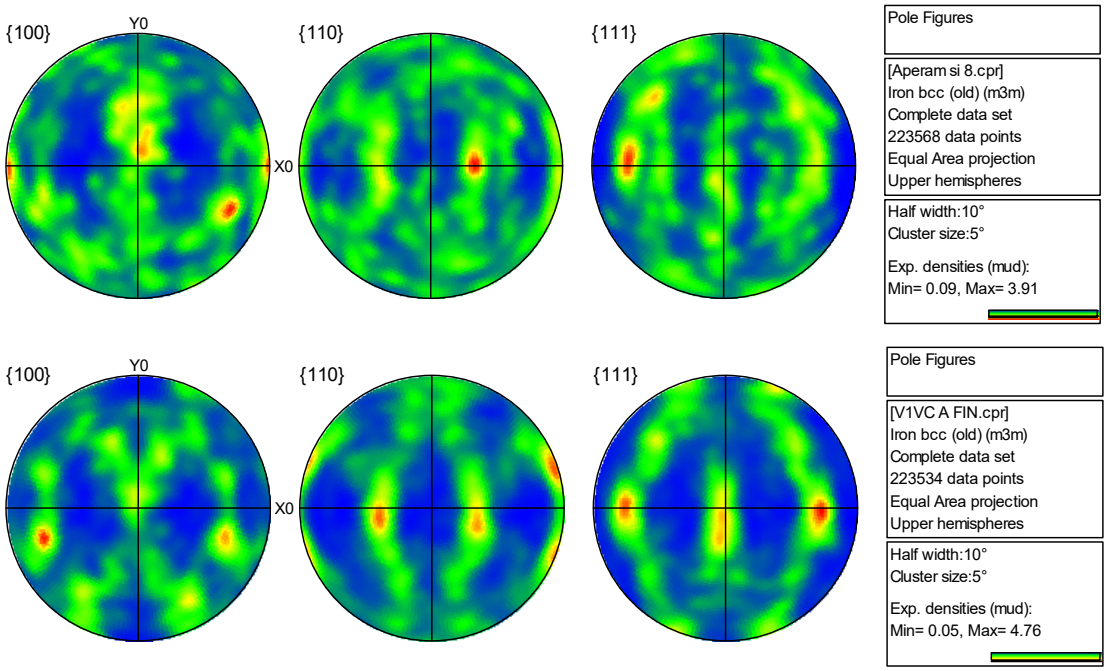

Figure 12. Above: pole figure of basic material, 0A, after cold rolling and final annealing. Below: pole figure of modified material, 1C, after cold rolling and final annealing.

Figure 13a shows the band contrast (BC), coincidence site lattice (CSL) and grain boundaries (GB) map, Fig. 13b shows the CSL legend, while Fig. 13c shows the GB legend of basic and modified material in samples after such cold rolling and final annealing. The characterisation reveals the presence of retained martensite in the basic material with a content of 29 %, which does not appear in the modified one (data processing as in Figs. 6 and 10).

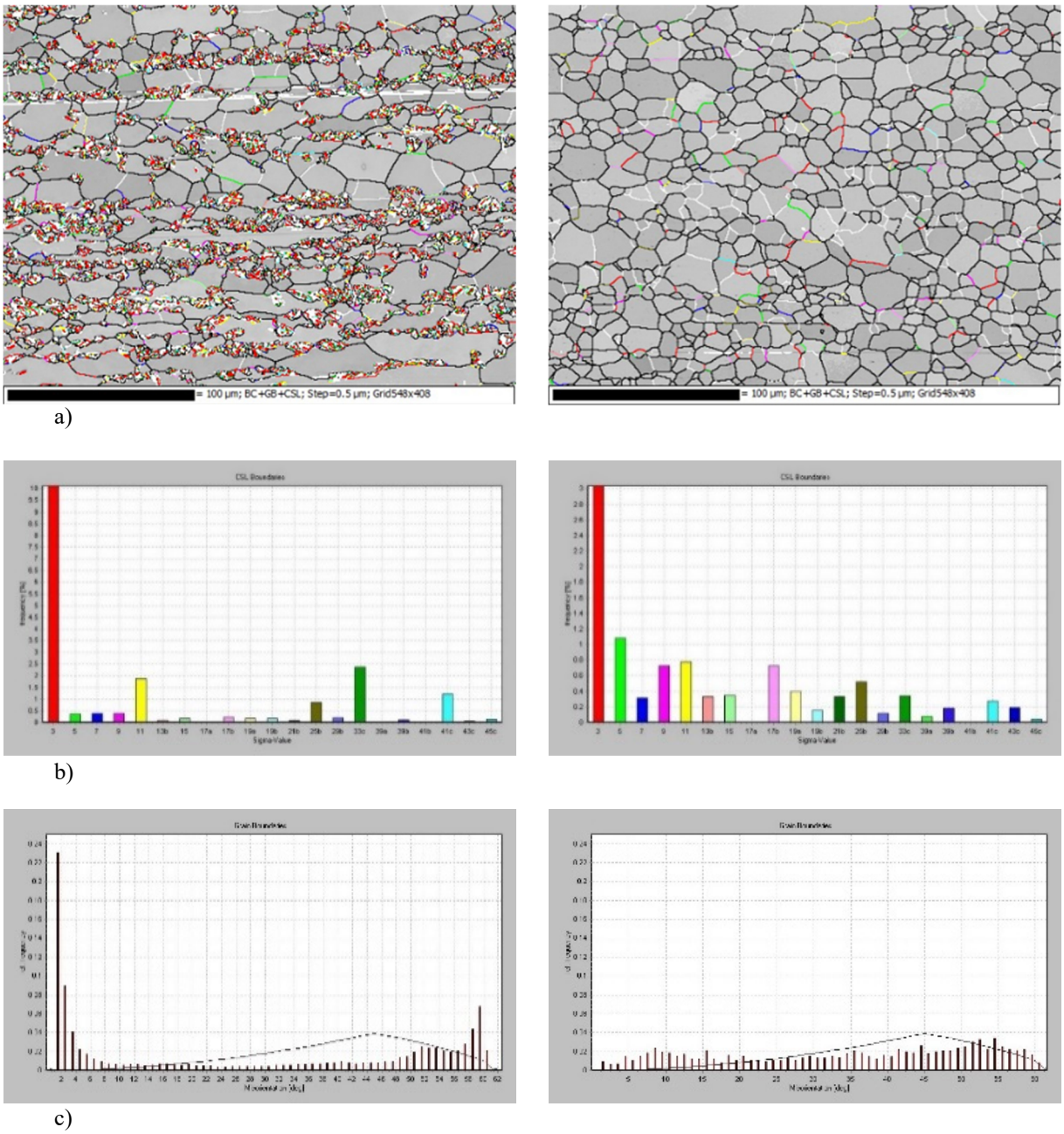

Figure 13. a) Band contrast (BC), coincidence site lattice (CSL) and grain boundary (GB) map of basic material, 0A (left) and modified material, 1C (right) after final annealing. b) CSL legend of basic (left) and modified (right) material in samples after final annealing. c) GB legend of basic (left) and modified (right) material after final annealing.

4. Conclusions

- The macrostructures indicate that the solidification mechanism is heterogeneous in the material with basic composition, while in the modified composition, it is homogeneous. As well, sub-grains are revealed in the basic composition material but not in the modified one.

- Mechanical tests show that the materials after hot rolling present small deformation resistance, but after final annealing a basic composition sheet exhibits more pronounced anisotropy and lower deep drawability than the modified composition one.
- γ-fibre increases with processing progress in both materials, from hot rolling to final annealing, although this fibre is developed strongly in the modified steel after final annealing, while the α-fibre was mostly found in the basic one.
- Lankford coefficients and EBSD results confirm the evolution of texture through the manufactured processing of ferritic stainless steel, mainly in the material with modified composition.
- In addition, the characterisation reveals the presence of a phase in the ferrite matrix, identified as martensite, higher in the basic material in the initial stages of the processing route with respect to the modified material and that are not present in the modified composition after final annealing.
- As a result, the modified composition and process delivers a better re-crystallisation status and thus the best drawability performance.

References

[1] Kim J and Tasan C C 2019 *Int. J. Hydrogen Energy* **44** 6333-6343
[2] Sornin D L, Karch A and Logé R E 2018 *J. Mater. Sci.* **53** 2965-2975
[3] Alturk R, Mates S, Xu Z and Abu-Farha F 2017 in: *TMS 2017 146th Annual Meeting & Exhibition Supplemental Proceedings*. (Springer Int. Publ.) 243-254
[4] Raabe D and Lücke K 1993 *Mater. Sci. Technol.* **9** 302-311
[5] Kestens L A I and Pirgazi H 2016 *J. Mater. Sci. Technol.* **32,** 1303-1315
[6] Gurao N P and Satyam Suwas 2016 *Metall. Mater. Trans. A* **48** 809-827
[7] Herrera C, Ponge D and Raabe D 2008 *Steel Res. Int.* **79** 482-488
[8] Gobernado P, Petrov R H, Moerman J, Barbatti C and L A I Kestens 2012 *Mater. Sci. Forum* **702-703** 790-793
[9] Aparecida K, Brandao D and Reis de Oliveira T 2018 *Mater. Res.* **21** e20170873
[10] Starink M J 2017 *Mater. Sci. Engng. A* **705C** 42-45
[11] Khatirkar R K, Nimsarkar S, Das P, Vishwakarma A and Thawale N 2010 *Trans. Indian Inst. Metals* **63** 55-62
[12] Gonçalves R J, Gomes D, Batista H J, Reis T and Mendonça B 2017 *Mater. Res.* **20** 1593-1599
[13] He Y, Jin H, Chu Y, Chen J, Zhang Z, Huang H and Wang J 2017 *Trans. Mater. Heat* **38** 83-90
[14] Zhang C, Zhang L, Shen W, Xia Y and Yan Y 2017 *Acta Metallurgica Sinica* **30** 79-88
[15] Gao F, Yu F, Misra R, Zhang X, Zhang S and Liu Z 2015 *J. Mater. Engng. Performance* **24** 3862-3880
[16] Gobernado P, Petrov R H, Ruiz D, Leunis E and Kastens I 2010 *Adv. Engng. Mater.* **12** 1077-1081
[17] De Cock T 2009 *Thesis*. (Madrid, Spain: Universidad Complutense de Madrid)
[18] Ma X, Zhao J, Du W, Zhang X and Jiang Z 2018 *Mater. Characterization* **137** 201-211
[19] Oliveira A, Magalhaes C, Silva D, Oliveira A, Dutra I and Brandao D 2016 *J. Mater. Res* **31** 2838-2849
[20] Galán R 2013 *Engineering Degree Master*. (Cádiz, Spain: Universidad de Cádiz)
[21] Serenelli M, Bertinetti M and Signorelli 2014 *Rev. Iberoamericana Ing. Mecánica* **18** 75-85
[22] Herrera C, Lima N B, Ferreira A, Plaut R L and Padilha A F 2009 *J. Mater. Processing Technol.* **209** 3518-3524
[23] Hutchinson W B 1984 *Int. Metals Rev.* **29** 25-42
[24] Gao Z, Li J and Wang Y 2018 *Steel Res. Int.* **1800397** 1-9
[25] Ennis B L, Bos C, Aarnts M P, Lee P D and Jimenez-Melero E 2018 *Mater. Sci. Engng.* **713** 278-286
[26] Presslinger H, Mayr M, Tragl E and Bemhard C 2002 *Steel Res. Int.* **77** 107-115
[27] Núñez A, Llovet X and Almagro J F 2013 *Microsc. Microanal.* **19** 959-968

[28] Suwas S and Kumar Ray R 2014 Crystallographic texture of materials. in: *Engineering Materials and Processes*. (New York, NY: Springer)
[29] Oxford Instruments 2016 *AZtec Reclassify Phase*. Application note. (High Wycombe, UK: Oxford Instruments)
[30] Oxford Instruments 2013 *Band refinement*. Technical Bulletin. (High Wycombe, UK: Oxford Instruments)
[31] Wilkinson A J, Meaden G and Dingley D J 2006 *Ultramicroscopy* **106** 303-313
[32] Maurice C and Fortunier R 2008 *J. Microscopy* **230** 520-529
[33] Oxford Instruments 2012 *AZtec Tru-I*. Application note. (High Wycombe, UK: Oxford Instruments)
[34] Oxford Instruments 2011 *AZtecHKL - In depth*. Application note. (High Wycombe, UK: Oxford Instruments)
[35] Lu H-H, Li W-Q, Du L-Y, Guo H-K, Liang W, Zhang W-G and Liu Z-G 2019 *Mater. Sci. Engng. A* **754** 502-511
[36] Mehtonen S, Karjalainen L and Porter D 2013 *Mater. Sci. Engng. A* **571** 1-12
[37] Krauss G 2017 Review. *Steel Res. Int.,* **88**